Mater Renew Sustain Energy (2015) 4:12
DOI 10.1007/s40243-015-0055-8

ORIGINAL PAPER

Limitations of ultra-thin transparent conducting oxides for integration into plasmonic-enhanced thin-film solar photovoltaic devices

Jephias Gwamuri[1] · Ankit Vora[2] · Rajendra R. Khanal[3] · Adam B. Phillips[3] · Michael J. Heben[3] · Durdu O. Guney[2] · Paul Bergstrom[2] · Anand Kulkarni[2] · Joshua M. Pearce[1,2]

Received: 20 April 2015 / Accepted: 3 July 2015 / Published online: 16 July 2015

Abstract This study investigates ultra-thin transparent conducting oxides (TCO) of indium tin oxide (ITO), aluminum-doped zinc oxide (AZO) and zinc oxide (ZnO) to determine their viability as candidate materials for use in plasmonic-enhanced thin-film amorphous silicon solar photovoltaic (PV) devices. First a sensitivity analysis of the optical absorption for the intrinsic layer of a nano-disk patterned thin-film amorphous silicon-based solar cell as a function of TCO thickness (10–50 nm) was performed by simulation. These simulation results were then used to guide the design of the experimental work which investigated both optical and electrical properties of ultra-thin (10 nm on average) films simultaneously deposited on both glass and silicon substrates using conventional rf sputtering. The effects of deposition and post-processing parameters on material properties of ITO, AZO and ZnO ultra-thin TCOs were probed and the suitability of TCOs for integration into plasmonic-enhanced thin-film solar PV devices was assessed. The results show that ultra-thin TCOs present a number of challenges for use as thin top contacts on plasmonic-enhanced PV devices: (1) optical and electrical parameters differ greatly from those of thicker (bulk) films deposited under the same conditions, (2) the films are delicate due to their thickness, requiring very long annealing times to prevent cracking, and (3) reactive gases require careful monitoring to maintain stoichiometry. The results presented here found a trade-off between conductivity and transparency of the deposited films. Although the sub 50 nm TCO films investigated exhibited desirable optical properties (transmittance greater than 80 %), their resistivity was too high to be considered as materials for the top contact of conventional PV devices. Future work is necessary to improve thin TCO properties, or alternative materials, and geometries are needed in plasmonic-based amorphous silicon solar cells. The stability of ultra-thin TCO films also needs to be experimentally investigated under normal device operating conditions.

Keywords Transparent conducting oxide (TCOs) · Plasmonics · Solar photovoltaics · Indium tin oxide · Zinc oxide · Aluminum-doped zinc oxide

Introduction

Despite the material, sustainability, economic and technical benefits of thin-film solar photovoltaic (PV) devices [1–3], conventional crystalline silicon (c-Si) modules dominate the market [4]. The cost of c-Si PV has fallen to the point that the balance of systems (BOS) and thus the efficiency of the modules plays a major role in the levelized cost of electricity for solar [5]. There is thus a clear need to improve the efficiency of thin-film devices further [6]. Recent developments in plasmonics theory promise new methods with great potential to enhance light trapping in thin-film PV devices [7–14]. To fully exploit these

✉ Joshua M. Pearce
pearce@mtu.edu

[1] Department of Materials Science and Engineering, Michigan Technological University, 1400 Townsend Dr., Houghton, MI 49931-1295, USA

[2] Department of Electrical and Computer Engineering, Michigan Technological University, 1400 Townsend Dr., Houghton, MI 49931-1295, USA

[3] Wright Center for Photovoltaic Innovation and Commercialization, Department of Physics and Astronomy, School of Solar and Advanced Renewable Energy, University of Toledo, Toledo, OH 43606, USA

potential benefits offered by plasmonic-based devices, TCOs with high transmittance (low loss) and low enough resistivity are to be used as device top contacts. However, for current transparent conducting oxides (TCOs) to be successfully integrated into the novel proposed plasmonic-enhanced PV devices, ultra-thin TCOs films are required [14]. For example, simulations by Vora et al. showed a 19.65 % increase in short circuit current (J_{SC}) for nano-cylinder patterned solar cell (NCPSC) in which the ITO layer thickness was kept at 10 nm to minimize the parasitic Ohmic losses and simultaneously act as a buffer layer while helping to tune the resonance for maximum absorption [14]. TCOs such as the most established indium tin oxide (ITO), aluminum-doped zinc oxide (AZO) and zinc oxide (ZnO) are standard integral materials in current thin-film solar PV devices [15–18]. Bulk material properties for common TCOs including ITO have been well researched and documented for different processing conditions and substrates [15, 16, 19–23]; however, this is not the case for ultra-thin TCOs. The few exceptions include Sychkova et al. [24], who reported both optical and electrical properties of 9–80 nm ITO films deposited by pulsed DC sputtering varied with thickness and showed a general increase in resistivity with decrease in film thickness [24]. Other notable studies on ultra-thin ITO films using various deposition techniques include the following: Chen et al. who used filtered cathodic vacuum arc (FCVA) to deposit 30–50 nm on heated quartz and Si substrates [25]; Tseng and Lo, who used DC magnetron sputter for 34.71–71.64 nm ITO film on PET (polyethylene terephthalate) [26]; Kim et al. who used RF magnetron sputter for films between 40 and 280 nm deposited on PMMA substrate heated at 70 °C [27]; Alam and Cameron, who used sol–gel process for 50–250 nm film deposited on titanium dioxide film [20]; and Betz et al. who used planar DC magnetron sputtering for 50, 100 and 300 nm films on glass substrates [28]. The results from these few thin TCO studies reveal a pattern in which resistivity increases rapidly as film thickness decreases from 50 to 10 nm.

The electrical properties of ITO thin films depend on the preparation method, the deposition parameters used for a given deposition technique and the subsequent heat treatments. Key factors for the low resistivity have not been clearly documented because of the complex structure of the unit cell of crystalline In_2O_3 formed by 80 atoms and the complex nature of the conducting mechanisms in polycrystalline films [29]. The issue is further complicated by the large number of processing parameters, even for a single technique.

To probe these challenges and to determine if ITO, AZO and ZnO are viable candidate materials for use in plasmonic-enhanced thin-film PV devices, sensitivity analysis on TCO thickness (10–50 nm) versus absorption was performed using COMSOL Multiphysics RF module v4.3b on the optical absorption in the i-a-Si:H layer of nano-disk patterned thin-film a-Si:H solar cells (NDPSC) shown in Fig. 1a [15]. These simulation results are used to guide the experimental work which investigated both optical and electrical properties of ultra-thin (10 nm on average) films simultaneously deposited on both glass and silicon substrates (with a thermally grown oxide layer. The effects of deposition and post-processing parameters on material properties of ITO, AZO and ZnO ultra-thin TCOs were probed and the suitability of TCOs for integration into plasmonic-enhanced thin-film solar PV devices was assessed. From these results some of the limitations of thin TCOs for plasmonic optical enhancement of thin-film PV were identified.

The optical effects of TCO thickness

Sensitivity analysis for the proposed silver nano-disk patterned solar cell (NDPSC) was performed in the 300–750 nm spectral range to determine the optimum ITO layer thickness which would promote maximum enhancement and minimize Ohmic losses. Having a TCO spacer layer with as low as possible Ohmic losses is desirable for efficient coupling of light from the silver nano-discs into the active layers of the device. The results are shown in Fig. 1b and theoretically show 10 nm films offer the best absorption and hence the greatest potential to improve efficiency in plasmonic-based PV devices. From these results, AZO and ITO offer the best potential due to lower Ohmic losses and ZnO, despite having the greatest Ohmic losses among the three TCOs, is still promising particularly for the sub 20 nm films since its absorption (>250 W/m^2) is still higher than that expected of a standard PV device.

Experimental details

The focus of the study was to investigate ways of improving material properties of ultra-thin TCOs for integration into plasmonic-enhanced thin-film solar PV devices by studying the effects of different process parameters on both optical and electrical properties of sub 50 nm films. A comparative study of the three most commonly used TCOs in thin-film commercial solar cells is undertaken, and a more in-depth study of ITO is performed.

Sample preparation and fabrication

Samples of ITO with thickness ranging from 10 to 50 nm were deposited on both glass and n-doped silicon (with a 32-nm thermally grown oxide layer) substrates using rf sputter deposition techniques previously described in refs

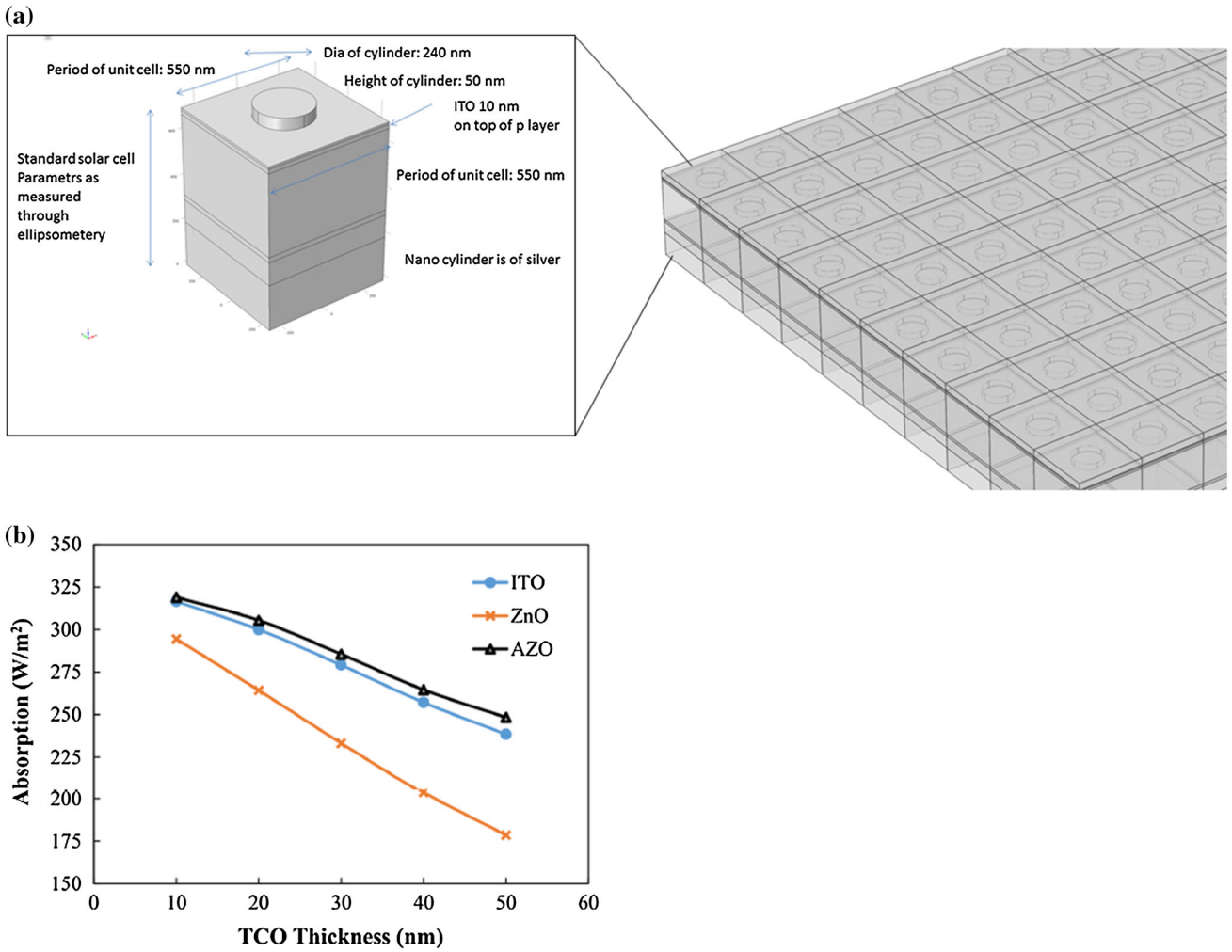

Fig. 1 **a** Structure of the NDPSC with an enlarged unit cell, **b** absorption as a function of ITO, ZnO and AZO thickness. The results simulated using COMSOL show how the useful optical absorption in the active regions of plasmonic PV devices varies with TCO type and thickness. Theoretically, at small film thicknesses Ohmic losses decrease and useful optical absorption increases [15]

[30–32]. A 99.99 % 4-inch pressed ITO (Sn_2O:In_2O_3 10:90 % wt) target was used, and an average base pressure of 7×10^{-8} torr was achieved before deposition. Both the glass and silicon substrates were ultrasonically cleaned in isopropanol for 5 min. All other process parameters such as target bias [900 V (ITO and ZnO) and −500 V (AZO)] and substrate distance (75 mm) were kept constant through the experiment. Substrates and target were sputter pre-cleaned in an argon environment for 5 min before each run. The protocol for pre-cleaning is described in Ref. [29]. To investigate substrate dependency, ITO was deposited on a pair of substrates for 1 min with 0 % oxygen ratio and 100 W rf power. ZnO samples were processed at rf power of 100 W on glass and silicon substrates in an argon environment and 0 % oxygen in the same system as ITO using a stoichiometric 99.99 % 4-inch pressed ZnO target. The process pressure was maintained at 7.1×10^{-3} torr and the deposition rate was calculated to be 8 nm/min.

AZO was processed using a Perkin–Elmer Model 2400-8 J rf sputter deposition system using an 8-inch (203.2 mm) target. The rf power was kept at 500 W, argon flow rate at 18.0 sccm, oxygen rate of 2.0 sccm and process pressure at 7.3×10^{-3} torr. The system was initially pumped to a base pressure of 6.0×10^{-8} torr. The process parameters are summarized in Table 1.

To investigate the effects of post-processing treatment on both optical and electrical effects, additional samples of ITO films on sodalime glass (SLG) substrates were processed using a different instrument [33] to obtain a pair of film samples with varying thicknesses from 10 to 50 nm in steps of 10 nm. The system is a four-gun sputtering system with a target to substrate spacing of approximately 4″. An ITO (90 % In_2O_3/10 % SnO_2 from Lesker) target was used. The material was sputtered using 100 W rf under 4 mTorr of Ar. Deposition time was varied for film thickness with 36 s resulting in 10 nm (∼3 A/sec). This deposition rate

Table 1 Summary of process parameters for the TCOs

Sample name	TCO	Substrate type	RF power (W)	Target bias (V)	Process gases flow rates (sccm)		Film thickness (nm)
					Ar	O_2	
0A	ITO	Glass	100	900	10	0	9.55
0B		Si/SiO_2					10.02
$1A_1$		Glass					19.92
$1A_2$		Si					19.75
1B		Glass					10.23
1C							20.01
1D							30.79
1E							39.70
1F							50.03
$2A_1$	ZnO	Glass					9.51
$2A_2$		Si/SiO_2					10.05
2B							20.01
2C							29.72
2D							38.98
2E							48.31
3A	AZO	Glass	500	500	18.0	2.0	12.16
3B		Si/SiO_2					11.93
3C							20.39
3D							30.04
3E							40.63

was determined by depositing for a set amount of time and measuring the resulting film thickness using stylus profilometry (Veeco Dektak 150).

One sample for each as-deposited pair was divided into three samples using a diamond scriber. The three pieces were then annealed separately at 400 °C for 10, 20 and 30 min, respectively, using UHP forming gas (FG) (95 % N_2/5 % H_2 from Air Gas) in a sealed (by vacuum coupling components) quartz tube inside a tube furnace. The furnace was equilibrated at the heating temperature prior to sample introduction. The samples were placed in the quartz tube; then the tube was purged with FG at 5 scfm for 5 min—this was approximately four exchanges of tube volume. After purging, the samples were introduced into the hot zone with a vacuum-sealed push rod, and the flow rate was reduced to approximately 150 sccm for the duration of heating. After heating, the samples were removed from the hot zone and cooled by increasing the gas flow. After characterization, the sample previously annealed at 400 °C for 30 min was further annealed at 500 °C for 10 min.

Optical and electrical characterization process

The film thickness measurements and optical characterization were carried out using spectroscopic ellipsometry (J.A Woollam Co UV–VIS V-VASE with control module VB-400). In each case, a standard scan was performed ranging from 300 to 1000 nm in increments of 10 nm for the 65°, 70° and 75° incident angles. Random detailed scans were performed for the quality check purposes although they are normally not necessary for isotropic samples. Ellipsometry analysis was performed following the process by Synchkova [24]. Intensity measurements were carried out using the VASE for normal transmission incidence (0° reflection angle) for the three TCOs on glass substrates for the same wavelength range as above. A baseline scan was obtained for the clean SLG substrate first followed by the main data scans using baseline data. Both the baseline and the data scans were acquired in close successions to minimize errors due to light source intensity fluctuations.

Electrical characterization was performed using a four-point probe system consisting of ITO optimized tips consisting of 500 micron tip radii set to 60 g pressure and an RM3000 test unit from Jandel Engineering Limited, UK. The sheet resistance of the 10 and 20 nm TCOs on glass and on silicon substrates with a spacer oxide layer was determined by direct measurement for both forward and reverse currents. For each TCO on glass sample, a mean sheet resistance value from three random points was used in the final results whilst a mean of only two points was used for the TCO on Si samples since they were smaller.

All samples were imaged for film quality and a compositional analysis was done using a Hitachi S4700 field emission scanning electron microscope (FE-SEM). Atomic force microscopy (AFM) was performed using a Veeco Dimension 3000 equipment with cantilever tips (Tap300Al-G) on a 1:1 acquisition aspect ratio. The field of view was 2 μm at 512 pixel width and scans performed at a speed of 0.5 Hz. Three randomly selected fields of view were acquired per sample and the analyzed areas were limited near to the center of the sample. Roughness analysis was then performed on a defect-free region.

Theory and calculations

The theoretical derivations of both the resistivity and attenuation coefficient of the ITO films are highlighted in Sects. 3.1 and 3.2 below to explain the underlying processes contributing to the results reported in this paper.

Resistivity measurements

Sheet resistance measurement was used to obtain the resistivity:

$$R = \frac{\rho L}{tW} = R_s \frac{L}{W}, \quad (1)$$

where R is the resistance, R_s is the sheet resistance, and L, W and t are the sheet length, width and thickness, respectively.

As the film thickness is measured, the bulk resistivity ρ (in ohm cm) can be calculated by multiplying the sheet resistance by the film thickness in cm:

$$\rho = R_s \times t \quad (2)$$

Transmittance

To determine the true transmittance of the TCOs, it was necessary to perform a correction on the experimental data to compensate for losses due to both surface reflection and absorption due to the glass substrate. It is assumed light passing through the glass substrate undergoes attenuation according to Beer-Lambert's law:

$$I_g = I_o e^{-\alpha_g t_g}, \quad (3)$$

where I_0 and I_g represent the initial incident intensity and intensity through the glass substrate, α_g and t_g are the attenuation coefficient of the glass and glass thickness, respectively.

The total normalized transmittance, T is given by

$$T = 1 - A - R \quad (4)$$

where A and R represent the total absorbance and reflectance, respectively.

Results and discussion

TCOs characterization

The transmittance and resistivity measurement results for the TCOs are discussed below.

Transmittance

Figure 2 below shows how transmittance of the TCOs studied varied within the 300–1000 nm wavelength range.

Transmittance results support the sensitivity analysis results. For the 20-nm films, AZO has greater than 90 % transmittance for the 300–1000 wavelength range, whilst ITO and ZnO show an average transmittance greater than 80 and 70 %, respectively, in the same spectral range.

Sheet resistance

The resistivity of the 20 nm as-deposited TCO films on SLG substrates are shown in Table 2. ZnO, despite having the worst transmittance (Fig. 2), has the lowest resistivity among the three TCOs being compared here and AZO has the highest resistivity value. ITO has transmittance comparable to that of AZO and its resistivity is slightly higher than that of ZnO, making it the most promising candidate material for plasmonic-based devices.

Table 3 shows the dependence of ITO sheet resistance with substrate type and thickness. There was a marked difference between the readings on the 10- and 20-nm Si samples; however, there was no discernible difference between the readings on the 10 and 20 nm on glass. There were very small amounts of fluctuation which can be expected on high resistance samples, and it was more prominent on the Si samples. The readings reversed well, indicating that the film was uniform, with the worst correlation on the 10-nm Si sample. This is the limit of four-point probe capability. The 10-nm ITO on glass showed the

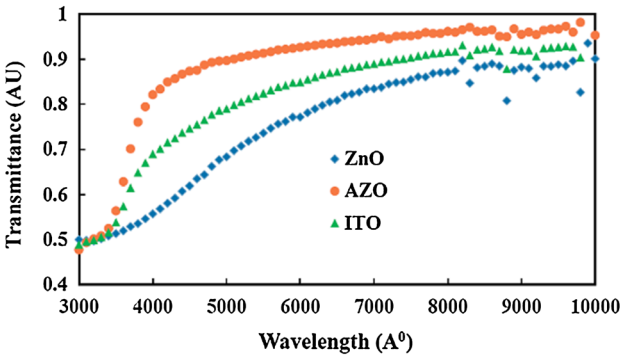

Fig. 2 Transmittance results for 20 nm thick ITO, ZnO and AZO films

Table 2 Resistivity of 20 nm as-deposited ITO, AZO and ZnO films on SLG substrates

Sample	Substrate	Thickness (nm)	Sheet resistance, R_s (Ω/□) × 10^3	Resisitivity, ρ (Ω cm)
ITO	Glass	20	623	1.3×10^{-3}
AZO	Glass	20	876	1.7×10^{-3}
ZnO	Glass	20	390	7.8×10^{-4}

Table 3 Sheet resistance of various as-deposited TCO samples

Sample	Substrate	Thickness (nm)	Input current	Sheet resistance, R_s (Ω/□) × 10^3	Resisitivity, ρ (Ω cm)
ITO	Glass	10	100 nA	830	8.3×10^{-4}
		20		623	1.3×10^{-3}
	Si	10	1 μA	422	4.2×10^{-4}
		20		83.9	1.7×10^{-4}

highest resistivity whilst the lowest resistivity value was recorded for the 20-nm Si substrate sample. The results are further confirmed by the nature of the microstructure observed by SEM (vide infra) for these samples.

ITO characterization

Transmittance measurements for ITO

Transmittance measurements for ITO samples deposited on SLG substrates are shown in Fig. 3. All transmittance values were normalized as given in Eq. (4). It can be noted that there is no discernible difference between the as-deposited and the heat-treated samples particularly for the 30-, 40- and 50-nm films. However, it is also interesting to note that for the 10- and 20-nm films, the as-deposited films have the highest transmittance with the 10-nm film being almost 100 % transmitting throughout the visible spectra. For the 40-nm film, annealing at 400 °C for 20 min gives the best transmittance. Generally it is observed that heat-treated ITO films in FG environment improve transmittance in the UV region of the spectra.

As-deposited thinner ITO samples (10 and 20 nm) have the transmittance greater than 95 %. It is interesting to note that the 40-nm film sample does not seem to follow this general trend, particularly the sample annealed for 20 min. This sample film shows the greatest increase in mean roughness (*vida infra*) when all other films' roughness is decreasing and it also has the best transmission for all the 40-nm film samples. The general trend is that the overall transmittance curve for the as-deposited ITO shifts down with increasing film thickness (i.e., the as-deposited film becomes less transparent with increasing thickness as expected). Around visible spectrum and at higher wavelengths, the transmittance for the as-deposited ITO approaches that of the annealed ITO (i.e., annealing is not much effective here in improving transparency). However, around UV wavelengths the transmittance for the as-deposited ITO shifts down below that of the annealed samples (i.e., at small wavelengths annealing is more effective as the annealed samples are more transparent). This is a well-known phenomenon (Burstein–Mess shift) which is a result of ITO optical band gap shifting towards higher energies when annealed in FG or H_2 gas. This is attributed to increase in carrier concentration and is well documented [25]. In addition, it appears that among the annealed samples, 20 min gives the optimum transmittance for thicknesses below 50 nm, especially at large wavelengths. There observed trend means that the use of thinner (10 nm), more transmitting and low loss (Ohmic losses) films will result in more light being coupled into the underlying i-a-Si:H layer rather than being absorbed in the TCO layer as is the case with thicker film (>20 nm).

Electrical characterization

Figure 4 shows the dependence of sheet resistance on film thickness, annealing temperature and time. Films annealed for 20 min give the lowest resistivity and show the same trend as those annealed for 30 min whilst the as-deposited resistivity versus thickness trend is similar to films annealed for 10 min. Results here show that annealing in FG lowers the resistivity. The lowest resistivity of approximately 4×10^{-4} Ωcm is for the 40-nm film annealed for 20 min. The highest resistivity value for the annealed samples is for the 20-nm film annealed for 10 min.

Film morphology and roughness

Effect of substrate on ultra-thin ITO films

Figure 5 shows results from SEM scans showing the surface morphology for both 10 and 20 nm as-deposited ITO

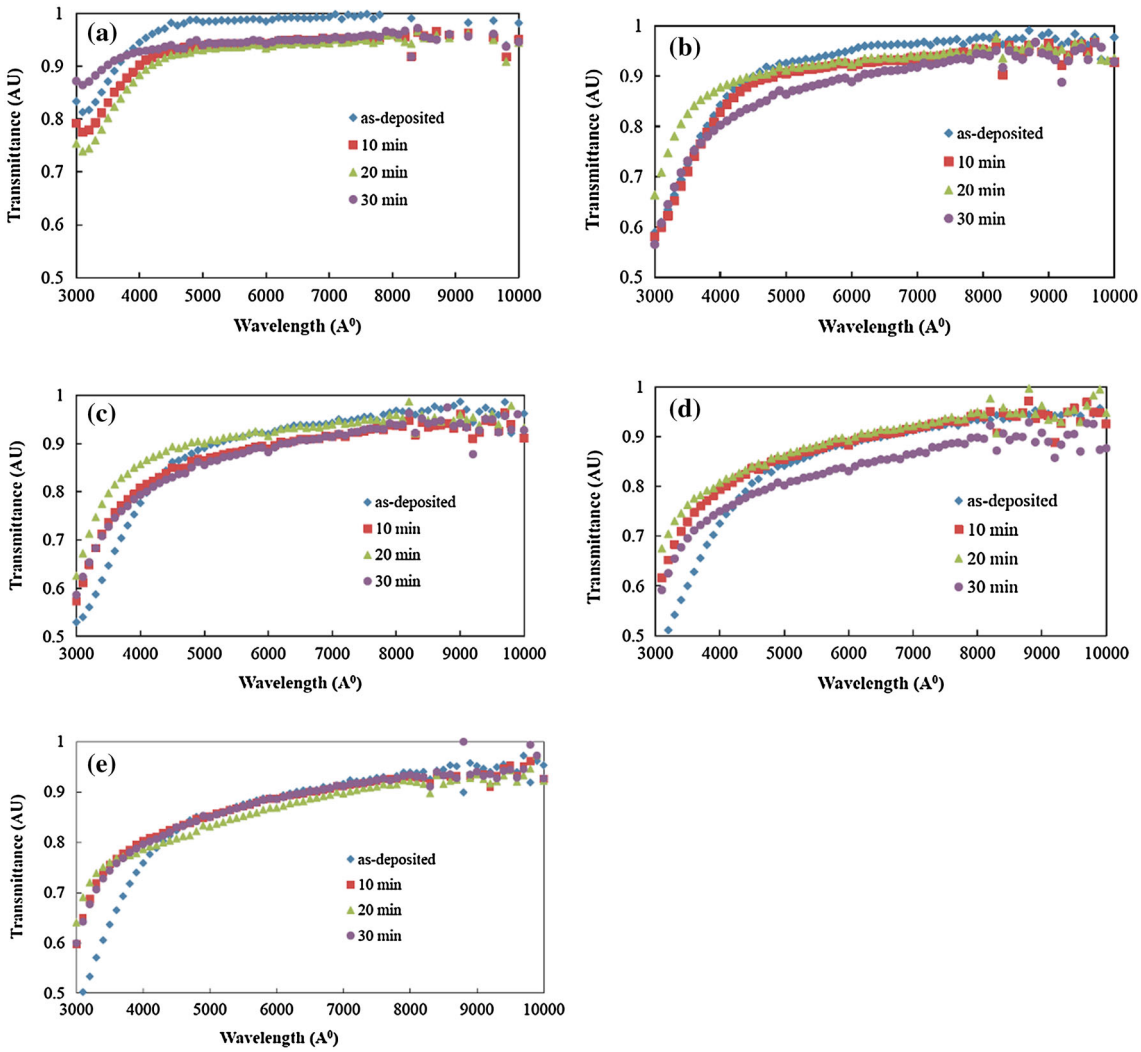

Fig. 3 Transmittance spectra for ITO as-deposited and annealed films on sodalime glass for **a** 10 nm, **b** 20 nm, **c** 30 nm, **d** 40 nm and **e** 50 nm ITO thickness

films. Figure 5a–c shows that the film surface is relatively smooth and predominantly amorphous in nature. Figure 5d shows signs of grains development. The AFM analysis results are shown in Fig. 6.

The results in Fig. 6 show how mean roughness values of ITO vary with substrate type and are in agreement with the results shown in Fig. 5. It can be observed in these images that ITO tends to form uniform features on silicon with no evidence of defects. This is not the case with ITO on glass substrate which, despite having finer features (10 nm film) exhibits some larger defects. These defects seem to increase with the increase in film mean roughness and thickness. Despite the presence of a few dust particles on the sample surface, results confirmed that the sputtered films were of good quality. The AFM roughness results are summarized in Table 4.

Effect of annealing time on ultra-thin ITO films

When ultra-thin ITO films were subjected to post-processing treatment at 400 °C in a FG environment, different treatment times produced different effects.

The as-deposited films mean roughness for this second batch of ITO samples were observed to vary between 0.67 and 0.85 nm. The 10-nm film had the smallest mean roughness value whilst the 20-nm film had the largest value. This may be due to the presence of surface defect features which seem to be more pronounced on the 20-nm

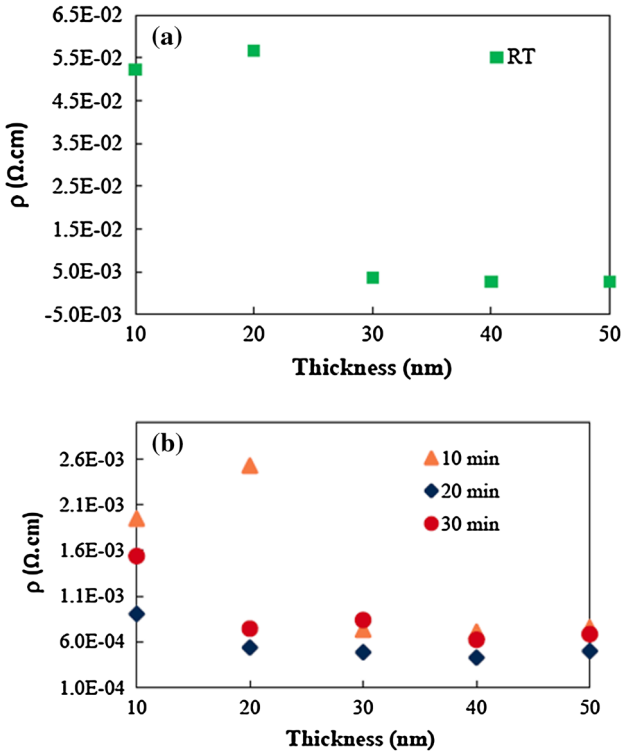

Fig. 4 Variation of resistivity with ITO film thickness for (**a**) as-deposited/room temperature (RT) (**b**) annealed films for 10, 20 and 30 min

film compared to all the other samples. Generally, all samples show a varying degree of dust particles' presence and potential artifacts. Sections of the film samples which exhibited heavy dust particles' (and any other contaminants) presence, striations and potential artifacts that were not consistent with other areas on the sample were excluded from the analysis.

The images show a sharp increase in the mean roughness for generally all films after 10 min of heat treatment. Whilst the film roughness is small for both the 10- and 20-nm films, it is observed to increase by a factor of two for the 30- to 50-nm film thickness samples. There is a trend for all films showing a decrease in mean roughness after 20 min of post-processing treatment with the 30-nm film showing the greatest decrease from approximately 1.9 to 1 nm. Evidently, annealing for 30 min results in a slight improvement in film roughness for the 30- to 50-nm range of film. However, the thinner films (10 and 20 nm) show great deterioration in film mean roughness when annealed for longer periods of time (30 min or greater). This can be explained by the onset of islands on both of these films. Island formation is more pronounced on the quasi 2D 10-nm film resulting in the mean roughness increasing from the initial value of approximately 0.7–1.9 nm.

The effects of annealing different ITO films in forming gas at 400 °C for 10, 20 and 30 min on films surface roughness are compared and summarized in Fig. 7.

The detailed study on ITO showed some dependency of electrical properties and surface roughness with substrate type which is consistent with results from previous studies on slightly thicker films. Also ITO films on glass show a high degree of surface defects and finer amorphous-like features which may explain the high and oscillating values of sheet resistance on these films. Films grown on Si substrate have uniform, but large features. However, the same films have higher resistivity values. All samples, as-deposited and annealed, have a transmittance value greater than 80 % with the as-deposited films being superior except for the 40-nm films for which the annealing for 20 min gives the best transmittance. Further analysis of samples shows films annealed for 20 min generally have the lowest resistivity and lower roughness values.

Future work is needed to improve other TCOs such as AZO and ZnO and to engineer new high-conductivity low-loss materials for integration into plasmonic devices. AZO exhibited a transmittance superior to that of ITO while ZnO had the best sheet resistance among the three TCOs being compared. Further investigative work is needed to find the balance between films with useful resistivity and acceptable Ohmic losses in plasmonic-based PV devices. Future work should focus on different processing techniques such as DC sputtering as well as exploring other post-processing environments.

Conclusions

Ultra-thin TCOs and in particular ITO present a number of challenges for use as thin top contacts on plasmonic-enhanced PV devices. First, both ultra-thin TCO optical and electrical parameters differ greatly from those of thicker (bulk) films deposited under the same conditions. Second, they are delicate due to their thickness, requiring very long annealing times to prevent film cracking. The reactive gases (usually oxygen or hydrogen) require careful monitoring to avoid over-oxidizing or over-reducing the film as it impacts their stoichiometry. There is a trade-off between conductivity and transparency of the deposited films. The sub 50 nm thick TCO films investigated exhibited desirable optical properties (transmittance greater than 80 %), which makes them viable for plasmonic PV devices

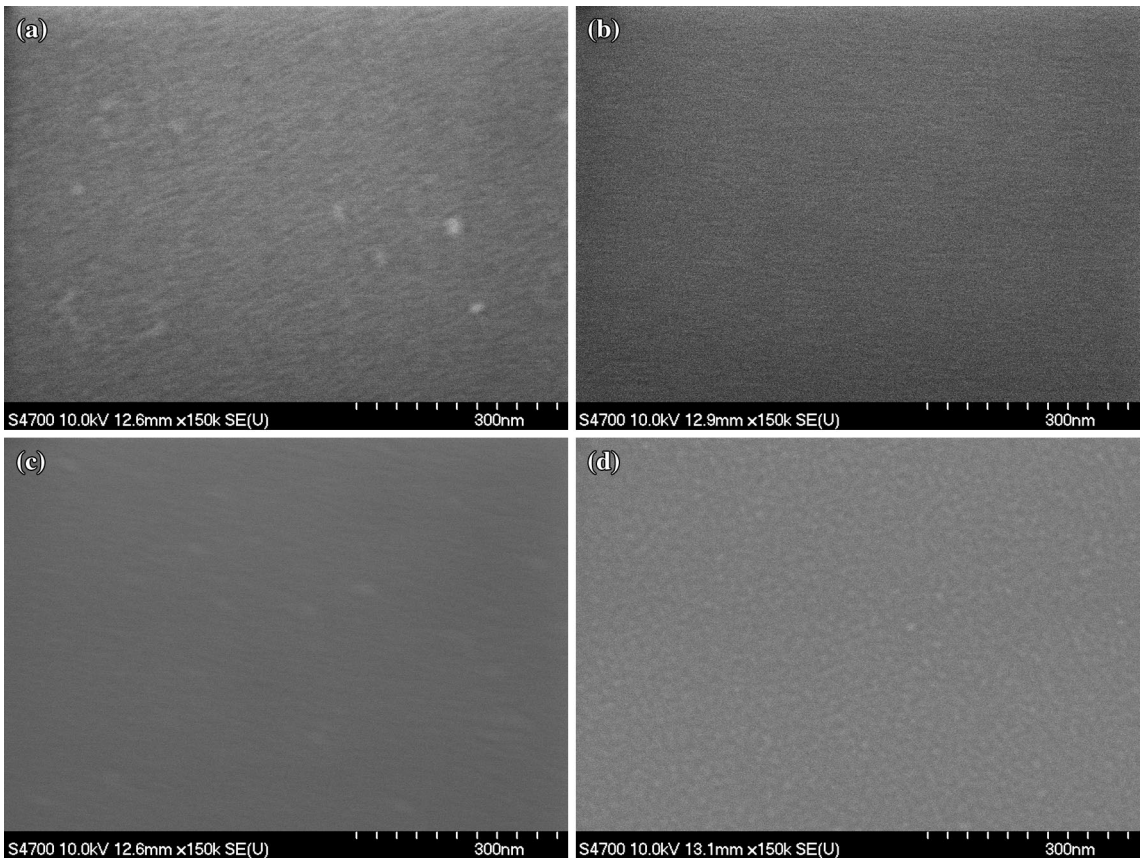

Fig. 5 FESEM images for (**a**) 10 nm ITO on glass, (**b**) 10 nm ITO on silicon (with oxide spacer), (**c**) 20 nm ITO on glass and (**d**) 20 nm ITO on silicon (with oxide spacer)

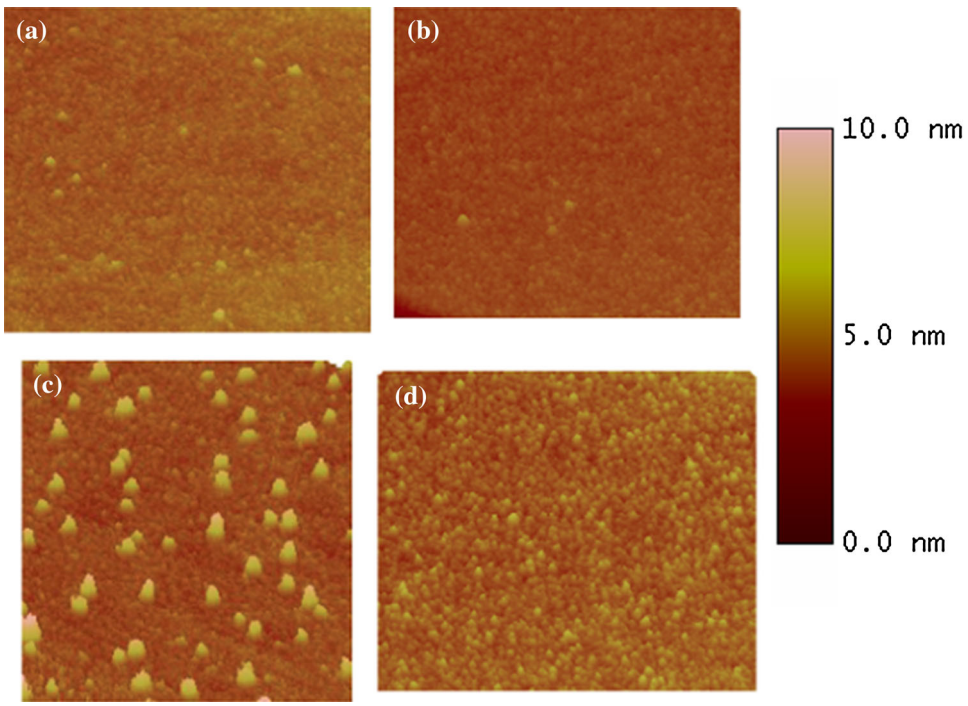

Fig. 6 AFM images for as-deposited (**a**) 10 nm ITO on glass, (**b**) 10 nm ITO on silicon (with oxide spacer), (**c**) 20 nm ITO on glass and (**d**) 20 nm ITO on silicon (with oxide spacer). *Image scale* is 10 nm

Table 4 Summary of AFM results for as-deposited ITO films on glass and Si substrates

Film	Roughness (nm)		Observations
	RMS roughness (Rq)	Mean roughness (Ra)	
ITO on Si wafer, 10 nm	0.44	0.35	Uniform, small features
ITO on Si wafer, 20 nm	0.58	0.45	Uniform features larger than 10 nm
ITO on glass, 10 nm	0.37	0.29	Very fine features with some larger defects
ITO on glass, 20 nm	0.83	0.52	Fine features with many large defects

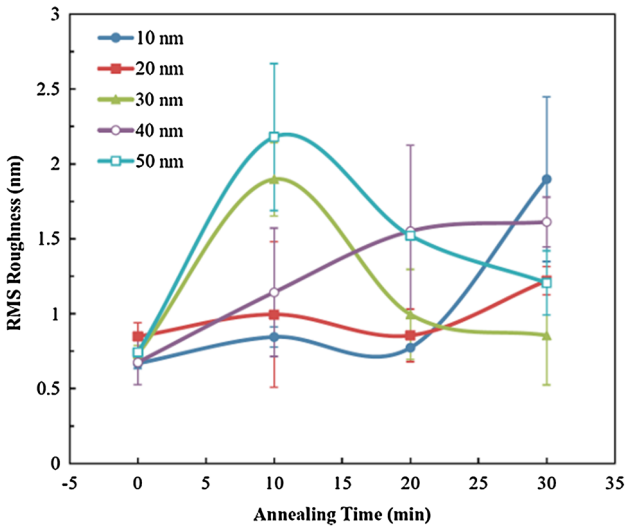

Fig. 7 RMS roughness of annealed ITO films. The figure shows a time series with an overlap of *error bars*

applications. However, all films evaluated here had resistivity values too high to be considered as materials for the top contact of conventional PV devices.

Acknowledgments Authors would like to acknowledge the support from faculty start-up funds from the University of Toledo, Fulbright (Science and Technology) funds, and the National Science Foundation (CBET-1235750). Furthermore, authors would like to acknowledge the helpful discussion with Dr. J. Mayandi.

References

1. Shah, A., Torres, P., Tscharner, R., Wyrsch, N., Keppner, H.: Photovoltaic technology: the case for thin-film solar cells. Science **285**(5428), 692–698 (1999)
2. Pearce, J.M.: Photovoltaics—a path to sustainable futures. Futures **34**(7), 663–674 (2002)
3. Fthenakis, V.: Sustainability of photovoltaics: the case for thin-film solar cells. Renew Sustain Energy Rev **13**(9), 2746–2750 (2009)
4. Saga, T.: Advances in crystalline silicon solar cell technology for industrial mass production. NPG Asia Mater **2**(3), 96–102 (2010)
5. Branker, K., Pathak, M.J.M., Pearce, J.M.: A review of solar photovoltaic levelized cost of electricity. Renew Sustain Energy Rev **15**(9), 4470–4482 (2011)
6. Green, M.A.: Thin-film solar cells: review of materials, technologies and commercial status. J Mater Sci Mater Electron **18**(1), 15–19 (2007)
7. Gwamuri, J., Güney, D.Ö., Pearce, J.M.: Advances in plasmonic light trapping in thin-film solar photovoltaic devices. In: Tiwari, A., Boukherroub, R., Sharon, M. (eds.) Solar cell nanotechnology, pp. 243–270. Wiley, Hoboken (2013)
8. Vora, A., Gwamuri, J., Pala, N., Kulkarni, A., Pearce, J.M., Güney, D.Ö.: Exchanging ohmic losses in metamaterial absorbers with useful optical absorption for photovoltaics. Sci Rep 4:4901 (2014)
9. Khaleque, T., Magnusson, R.: Light management through guided-mode resonances in thin-film silicon solar cells. J Nanophoton **8**(1), 083995 (2014)
10. Green, M.A.: Third generation photovoltaics: advanced solar energy conversion (Springer Series in Photonics). Springer (2005)
11. Atwater, H.A., Polman, A.: Plasmonics for improved photovoltaic devices. Nat Mater **9**(3), 205–213 (2010)
12. Maier, S.A.: Plasmonics: fundamentals and applications. Springer, New York (2007)
13. Maier, S.A., Atwater, H.A.: Plasmonics: localization and guiding of electromagnetic energy in metal/dielectric structures. J Appl Phys **98**(1), 011101 (2005)
14. McPeak, K.M., Jayanti, S.V., Kress, S.J.P., Iotti, S., Rossinelli, A., Norris, D.J.: Plasmonic films can easily be better: rules and recipes. ACS Photon **2**(3), 326–333 (2015)
15. Vora, A., Gwamuri, J., Pearce, J.M., Bergstrom, P.L., Güney, D.Ö.: Multi-resonant silver nano-disk patterned thin film hydrogenated amorphous silicon solar cells for Staebler-Wronski effect compensation. J Appl Phys **116**(9), 093103 (2014)
16. Kulkarni, A.K., Schulz, K.H., Lim, T.-S., Khan, M.: Electrical, optical and structural characteristics of indium-tin-oxide thin films deposited on glass and polymer substrates. Thin Solid Films **308**, 1–7 (1997)
17. Kulkarni, A.K., Schulz, K.H., Lim, T.S., Khan, M.: Dependence of the sheet resistance of indium-tin-oxide thin films on grain size and grain orientation determined from X-ray diffraction techniques. Thin Solid Films **345**(2), 273–277 (1999)
18. Leem, J.W., Yu, J.S.: Indium tin oxide subwavelength nanostructures with surface antireflection and superhydrophilicity for high-efficiency Si-based thin film solar cells. Opt. Express **20**(103), A431–A440 (2012)
19. Guillen, C., Herrero, J.: Comparison study of ITO thin films deposited by sputtering at room temperature onto polymer and glass substrates. Thin Solid Films **480**, 129–132 (2005)

20. George, J., Menon, C.S.: Electrical and optical properties of electron beam evaporated ITO thin films. Surf. Coat. Technol. **132**(1), 45–48 (2000)
21. Alam, M.J., Cameron, D.C.: Characterization of transparent conductive ITO thin films deposited on titanium dioxide film by a sol–gel process. Surf Coat Technol **142**, 776–780 (2001)
22. Houng, B., Wang, A.: Characterization of indium tin oxide films by RF-assisted DC magnetron sputtering. Appl. Surf. Sci. **258**(15), 5593–5598 (2012)
23. Thestrup, B., Schou, J., Nordskov, A., Larsen, N.B.: Electrical and optical properties of thin indium tin oxide films produced by pulsed laser ablation in oxygen or rare gas atmospheres. Appl Surf Sci **142**(1), 248–252 (1999)
24. Terzini, E., Thilakan, P., Minarini, C.: Properties of ITO thin films deposited by RF magnetron sputtering at elevated substrate temperature. Mater Sci Eng B **77**(1), 110–114 (2000)
25. Sytchkova, A., Zola, D., Bailey, L.R., Mackenzie, B., Proudfoot, G., Tian, M., Ulyashin, A.: Depth dependent properties of ITO thin films grown by pulsed DC sputtering. Mater Sci Eng B **178**(9), 586–592 (2013)
26. Cruz, L., Legnani, C., Matoso, I., Ferreira, C., Moutinho, H.: Influence of pressure and annealing on the microstructural and electro-optical properties of RF magnetron sputtered ITO thin films. Mater Res Bull **39**, 993–1003 (2004)
27. Chen, B.J., Sun, X.W., Tay, B.K.: Fabrication of ITO thin films by filtered cathodic vacuum arc deposition. Mater Sci Eng B **106**(3), 300–304 (2004)
28. Tseng, K.-S., Lo, Y.-L.: Effect of sputtering parameters on optical and electrical properties of ITO films on PET substrates. Appl Surf Sci **285**, 157–166 (2013)
29. Kim, D.-H., Park, M.-R., Lee, H.-J., Lee, G.-H.: Thickness dependence of electrical properties of ITO film deposited on a plastic substrate by RF magnetron sputtering. Appl Surf Sci **253**(2), 409–411 (2006)
30. Betz, U., Olsson, M.K., Marthy, J., Escolá, M.F.: On the synthesis of ultra smooth ITO thin films by conventional direct current magnetron sputtering. Thin Solid Films **516**(7), 1334–1340 (2008)
31. Tahar, R.B.H., Ban, T., Ohya, Y., Takahashi, Y.: Tin doped indium oxide thin films: electrical properties. J. Appl. Phys. **83**(5), 2631–2645 (1998)
32. Perkin-Elmer, R.F.: Sputtering System-6 Inch protocol: MOST. http://www.appropedia.org/Perkin-Elmer_RF_Sputtering_System-6_Inch_protocol:_MOST. Accessed 10 Jul 2015
33. Knickerbocker, S.A.: Ph.D. Dissertation, Michigan Technological University (1995)